Available online at www.sciencedirect.com
ScienceDirect
Physics of the Earth and Planetary Interiors 159 (2006) 32–42
PHYSICS OF THE EARTH AND PLANETARY INTERIORS
www.elsevier.com/locate/pepi

Acquisition of viscous remanent magnetization

Yongjae Yu *, Lisa Tauxe

Geosciences Research Division, Scripps Institution of Oceanography, La Jolla, CA 92093-0220, USA

Received 22 February 2006; received in revised form 23 May 2006; accepted 30 May 2006

Abstract

Viscous remanent magnetization (VRM) has been frequently suggested as a possible source of magnetic anomalies in ocean crust and as an important contributor of natural remanent magnetization in some volcanic and sedimentary rocks. Most references to VRM assume a linear dependence with log(t), yet long-term experimental data on VRM, while scarce often disagree with this simple notion. Here, we investigate the angular-dependence, grain-size dependence, initial-state dependence, and time (t) dependence of VRM acquisition. We observe a non-linear log(t) dependence of VRM acquisition over all time intervals (>10^4 s) for all the samples regardless of various experimental conditions. Echoing earlier studies, we also find that VRM acquisition is strongly dependent on the initial magnetic state of the samples. Samples in a thermally demagnetized initial-state were most susceptible to VRM acquisition. When VRM is produced parallel to the initial thermal remanence, VRM acquisition is negligible. VRM acquisition is more prevalent for magnetites in single-domain and multidomain (MD) grains than in the pseudo-single-domain range. In MD magnetites, frequent removal and restoration of samples (for the purpose of zero-field remanence measurement) apparently increases the efficiency of VRM acquisition.

Keywords: Viscous remanent magnetization (VRM); VRM acquisition; Magnetite; Log(t) relation; Grain-size

1. Introduction

Viscous magnetization (VM) or viscous remanent magnetization (VRM) is the isothermal change of the magnetization vector (**M**) with time t in the presence of an applied magnetic vector field (**B**). The distinction between VM and VRM is that VM is measured in the presence of a magnetic field, while the VRM is measured in the absence of an applied field (**B** = 0). Investigating VM is advantageous because of its continuity in measurements and because it is quick (e.g., Markert et al., 1976; Prévot, 1981; Tivey and Johnson, 1981, 1984; Dunlop, 1983). However, a VM experiment requires a major modification of readily available equipment (e.g., Le Goff and Gallet, 2004). The focus of the present study is on VRM.

VRM is ubiquitous in natural remanences and occasionally VRM is comparable in magnitude to or even larger than the primary natural remanent magnetization (NRM). As a result, VRM can obscure the faithful record of the ancient geomagnetic field. A significant role of VRM in the NRM has been observed in carbonates (Kligfield and Channell, 1981; Kent, 1985; Jackson and Van der Voo, 1986; Jackson, 1990; Kok and Tauxe, 1996a,b; Jackson and Worm, 2002), in iron ore (Shimizu, 1960), in loess/paleosol (Evans and Heller, 1994; Pan et al., 2001), in lunar rocks (Nagata and Carleton, 1970), in oceanic basalts/gabbros (Creer et al., 1970; Lowrie, 1973; Lowrie and Kent, 1976, 1978; Dunlop and Hale, 1977; Moskowitz and Banerjee, 1981; Prévot, 1981;

* Corresponding author.
E-mail address: yjyu@ucsd.edu (Y. Yu).

0031-9201/$ – see front matter © 2006 Elsevier B.V. All rights reserved.
doi:10.1016/j.pepi.2006.05.002

Smith, 1984; Gee et al., 1988; Pozzi and Dubuisson, 1992; Prévot and Bina, 1993; Bina and Prévot, 1994; Hall et al., 1995; Bowles and Johnson, 1999; Worm, 2001), in pelagic clays (Yamazaki, 1986; Yamazaki and Katsura, 1990), in peridotites (Bina and Henry, 1990; Lawrence et al., 2002), in red beds (Kent and Miller, 1987), in volcanic rocks (Biquand and Prévot, 1971; Smith and Verosub, 1994), and in volcanic seamount extrusives/intrusives (Gee et al., 1993). To provide a comparative physical basis for such NRMs, VRM has also been studied on sized synthetic (titano)magnetites (e.g., Walton, 1980; Özdemir and Banerjee, 1981; Tivey and Johnson, 1981, 1984; Dunlop, 1983; Sporer, 1984; Moskowitz, 1985; Worm et al., 1988; Muxworthy and Williams, 2006; Williams and Muxworthy, 2006). Detailed reviews are available in Dunlop (1973, 1983), Moskowitz (1985), and Bina and Prévot (1994).

Magnetic viscosity in rocks is thought to originate from thermal fluctuations. A formal equation for the growth of viscous magnetization for an ensemble of single-domain (SD) grains is

$$\mathbf{M}(t) = \mathbf{M}_{\mathrm{eq}} + (\mathbf{M}_0 - \mathbf{M}_{\mathrm{eq}}) \exp\left(-\frac{t}{\tau}\right) \quad (1)$$

where $\mathbf{M}_{\mathrm{eq}}$ is the magnetization at thermal equilibrium for field $\mathbf{B}$, $\mathbf{M}_0$ the magnetization at time $t = 0$, and τ is the relaxation time (e.g., Néel, 1949, 1955). In the paleomagnetic literature, acquisition of VM or VRM has been approximated as being proportional to $\log(t)$ (see reviews in Rimbert, 1959; Dunlop, 1973, 1983; Moskowitz, 1985; Bina and Prévot, 1994). On the basis of such a log-linear relationship, VRM acquisition is often expressed by the viscosity coefficient (S_{a}) that is defined as

$$S_{\mathrm{a}} = \frac{\partial \mathrm{M}}{\partial(\log(t))} \quad (2)$$

However, the validity of such an approximation has been shown to be false by many experimental results. For instance, a log-linear dependence has only rarely been documented in the past (e.g., Shimizu, 1960). In contrast, the acquisition characteristics of VRM are generally not linear with $\log(t)$ (e.g., Lowrie, 1973; Lowrie and Kent, 1978; Tivey and Johnson, 1981, 1984; Dunlop, 1983; Kelso and Banerjee, 1994). Note that such non-linear log-dependence occurs on many time scales (e.g., Dunlop and Özdemir, 1997; Fig. 10-1). For instance, a non-linear $\log(t)$ dependence of VRM acquisition in oceanic basalts occurred after only a few hundred hours (Lowrie, 1973) or after a few tens of hours (Lowrie and Kent, 1978). Furthermore, values of S_{a} are dependent on the details of experimental duration, temperature, state of initial magnetization, and angular relationship between VRM acquisition and the pre-existing remanence (e.g., Tivey and Johnson, 1981, 1984).

Although VRM has mostly been described entirely in terms of SD grains because the theoretical framework is more straightforward, VRM is quite commonly observed larger, more complexly magnetized grains (so-called pseudo-single-domain (PSD) or multidomain (MD) grains) as well. According to the interpretation of Néel (1950) for MD grains, a random internal magnetic field is added to the applied field as a result of irregular thermal excitations in domain walls. However, the theoretical treatment of VRM in MD grains is still a matter of debate (e.g., Moskowitz and Banerjee, 1981; Prévot, 1981; Dunlop, 1983; Smith, 1984; Sporer, 1984; Moskowitz, 1985; Gaunt, 1986; Williams and Walton, 1986, 1988; Kelso and Banerjee, 1994).

In the present study, we explore various aspects of acquisition of VRM experimentally. We examine the angular dependence, grain-size dependence, $\log(t)$ dependence, and the effect of initial magnetic state of sample on VRM acquisition. Our results are not easy to explain within the current theoretical framework and a new VRM theory is beyond the scope of the present study, nonetheless our observations should prove helpful for future revisions of VRM theory.

2. Prediction of VRM behavior from single-domain theory

To constrain better the characteristics of VRM, we wish to consider key features in VRM acquisition from a theoretical point of view. For mathematical convenience, we will consider only the Néel's version of SD theory (Néel, 1949). The relaxation time for uniaxial SD grains is

$$\frac{1}{\tau} = \frac{1}{\tau_0} \exp\left[-\frac{VM_{\mathrm{s}}B_{\mathrm{K}}}{2kT}\left(1 - \frac{B_0}{B_{\mathrm{K}}}\right)^2\right] \quad (3)$$

in which τ_0 ($\sim 10^{-10}$ s) is the atomic reorganization time, V is a grain volume, M_{s} the saturation magnetization, T the absolute temperature, B_0 the applied field, and B_{K} is the microscopic coercivity. Note that τ is extremely sensitive to changes in B_{K}, T and V.

According to Eqs. (1) and (3), VRM acquisition can be predicted if the detailed distribution of τ ($=f(\tau)$) is known as well as the initial (M_0) and equilibrium (M_{eq}) magnetizations. In order to predict the pattern of general VRM acquisition, we will numerically examine Eqs.

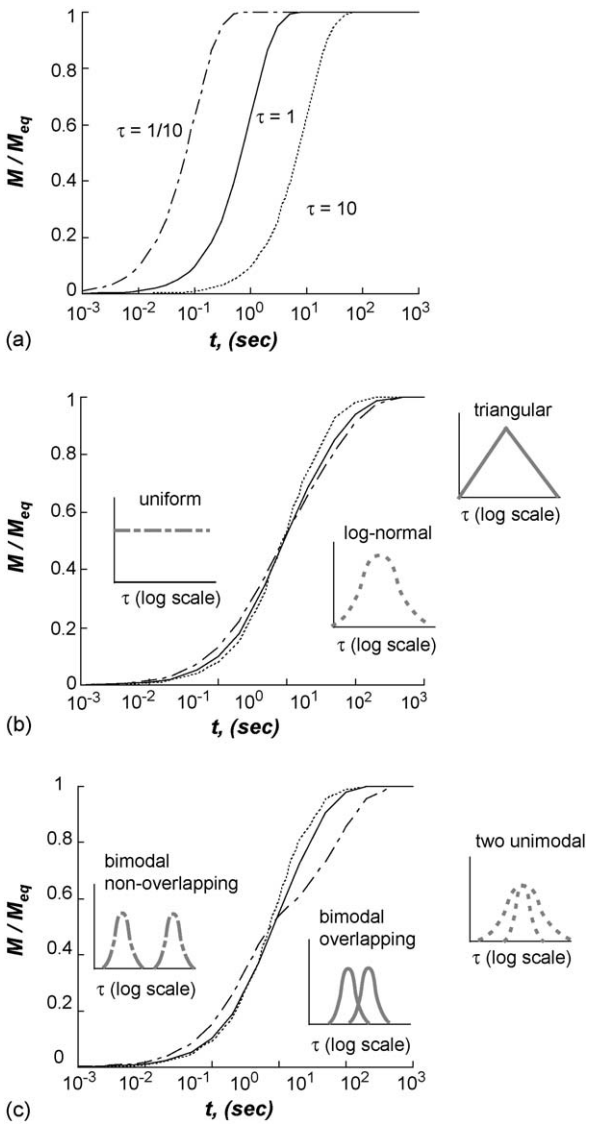

Fig. 1. (a) Magnetization as a function of time for a fixed τ (=0.1, 1, and 10). For $\tau = 1$, onset of blocking occurs at $t \sim 0.01\tau$ but saturates at $t \sim 8\tau$. (b, c) Comparison of VRM acquisition for various distribution of $f(\tau)$. VRM acquisition curves appear similar regardless of the detailed distribution of τ. Note that VRM acquisition is only linear with $\log(t)$ in the neighborhood of τ and a curved relationship to $\log(t)$ dominates in most time intervals.

(1) and (3). Consider the simplest case of a fixed τ with an initially demagnetized state ($\mathbf{M}_0 = 0$). For convenience, we consider the simple case of $\tau = 0.1$, 1, and 10 s (Fig. 1a). Magnetization increases as the time increases until the equilibrium magnetization is reached. Most of the growth occurs within a few orders of magnitude of the corresponding τ, including significant VRM acquisition for $t < \tau$. For example, growth of VRM begins at $t \sim 0.01\tau$ but the VRM is fully in equilibrium by $t \sim 8\tau$ for $\tau = 1$ s (Fig. 1a).

In nature, rocks contain magnetic particles with broad grain-size and shape distributions. Thus, we must consider representative distributions of τ that may exist in nature. Here, we consider three basic distributions: log-normal, triangular, and uniform (Fig. 1b). For simplicity, we set each distribution to span only two orders of magnitude with a mean at $\tau = 1$ s. In addition, we considered three more distributions (see Fig. 1c) that are combination of two log-normal distributions: (1) two non-overlapping distributions where each envelope follows a log-normal distribution spanning an order of magnitude with respective means at $\tau = 0.1$ and 10 s, (2) a bimodal overlapping distribution, and (3) unimodal distribution with two distribution widths.While values of τ in natural rocks are generally much larger and span more orders of magnitude than those considered here, key features displayed in Fig. 1 are of interest here:

(1) VRM acquisition curves appear similar regardless of the detailed distribution of τ (Fig. 1b and c); hence, the most important factor in VRM acquisition is the value of τ. The exact distribution of τ only results in differences in small details. In fact, this is to be expected considering the fact that changes in τ are only reflected logarithmically in magnetization. The only exception to this general behavior was the non-overlapping bimodal distribution modeled in Fig. 1c in which we observed a noticeable "hump" at $t \sim 1$.
(2) VRM acquisition at $t < \tau$ does not show a simple $\log(t)$ dependence (Fig. 1b and c). VRM acquisition is only linear with $\log(t)$ in the region very near τ itself; a curved relationship to $\log(t)$ dominates in most time intervals.

These theoretical predictions are well-known since the time of Néel (1949), yet few experimental results have been published that test them. Long time series of VRM behavior are rather rare (e.g., Lowrie and Kent, 1978; Gee et al., 1993) and those showed distinctively non-linear $\log(t)$ dependence. The overwhelming majority of published results have been interpreted in terms of log-linear behavior. Lowrie and Kent (1978) interpreted the long-term VRM behavior of Lowrie (1974) as a sequence of linear segments (see Fig. 2), although a single distribution of log-normally distributed values for τ (see inset of Fig. 2) and Eq. (1), fits the data remarkably well (dashed line). We attempt in this paper to provide a set of carefully controlled experiments with which to test the simple Néel theory of VRM acquisition.

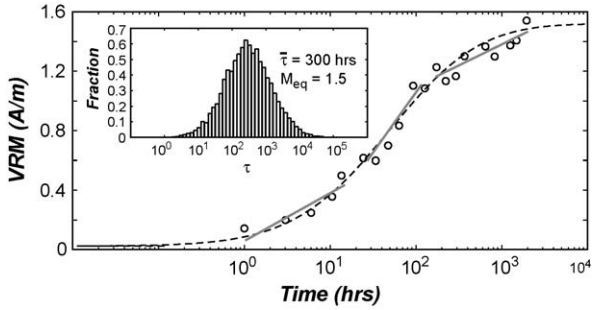

Fig. 2. Data from Lowrie (1974) with the "three-stage" interpretation using multiple linear segments as in Lowrie (1974) and Lowrie and Kent (1978) as solid lines. Also shown as a dashed line is the VRM according to Eq. (1) using the distribution of τ shown in the inset.

Table 1
Synthetic samples

Powder	d (μm)	q (aspect ratio)	Annealed magnetite	
			M_r/M_s	B_c (mT)
4000	0.065	1.48	0.195	18.47
Mapico	0.24	1.29	0.143	14.50
041183	18.3	1.57	0.017	2.06

Powders 4000 and 041183 are from the Wright Company. Powders Mapico is the product of Mapico Companies. d is the estimated grain-size and q is the average axial ratio. Size distribution was determined by counting individual grains from at least six different SEM photos per powder. See Yu et al. (2002) for details.

3. Samples

3.1. Synthetic samples

Three synthetic samples were prepared using commercial magnetite powders whose mean grain-sizes are 0.065 μm (SD), 1.06 μm (PSD), and 18.3 μm (MD) (Yu et al., 2002). Grain-sizes were determined using a Hitachi S-4500 scanning electron microscope (SEM). Detailed magnetic properties of these synthetic magnetites have been published elsewhere (Yu et al., 2002). Only a brief summary of rock magnetic parameters is given in Table 1.

For each powder, we prepared three sets of samples with varying volume concentrations of magnetite and different annealing conditions. For the first set, samples are ~0.5% by volume dispersions of magnetite in a matrix of CaF_2. Cylindrical pellets 8.8 mm in diameter and 8.6 mm in height were pressed and then tightly wrapped with quartz wool inside quartz capsules. The capsules were sealed under vacuum and annealed for 3 h at 700 °C to stabilize the magnetic properties. The second and third sets are annealed and unannealed bulk magnetite powders.

3.2. Natural samples

Five sets of magnetite-containing natural samples were also studied: three andesites (Yu, 1998) and twelve gabbros (Yu and Dunlop, 2001, 2002). The magnetic and paleomagnetic properties of the natural samples are well documented in corresponding references. A summary of rock magnetic properties of the samples used appears in Table 2. All the natural samples are cylindrical, 2.3 cm in diameter and 2.0 cm long.

Both for synthetic and natural samples, we used three sister specimens for each sample set. Sister samples are technically identical with one another. In particular, natural samples were chosen from a large collection of over 1000 specimens on the basis of their low magnetic anisotropy and their reproducible anhysteretic remanent magnetization (ARM) and thermoremanent magnetization (TRM) intensities (see Yu et al. (2002) for details). For instance, ARM and TRM were repeatedly produced six times over a period of 6 weeks. Intensities of ARM and TRM were reproducible within 3% to the initial ARM and TRM, respectively. In addition, principal components of the anisotropy of ARM (AARM) tensor are indistinguishable within 2%, suggesting their low degree of magnetic anisotropies.

4. Experiments

All the remanence measurements were carried out on a 2G Enterprises three-axis through-bore cryogenic magnetometer in the Scripps Paleomagnetic Laboratory. For alternating-field (AF) treatment, a Sapphire Instruments SI-4 AF demagnetizer with attached partial ARM acqui-

Table 2
Natural samples

Sample	n	Reference	T_{UB} (°C)	M_r/M_s	B_c (mT)	B_{cr} (mT)
Tudor Gabbro	6	[1]	580	0.37–0.44	35.2–41.5	58.2–65.2
An-ei Basalt	3	[2]	580	0.22–0.25	13.8–18.3	34.7–37.1
Cordova Gabbro	6	[3]	580	0.06–0.09	4.7–8.3	27.4–41.4

n: number of samples used in VRM experiments; [1] Yu and Dunlop (2001); [2] Yu (1998); [3] Yu and Dunlop (2002).

sition equipment was used. Measurements were carried out in a magnetically shielded space with an ambient field less than 250 nT. In addition, VRM acquisition was carried out in a hypernum can with an ambient field less than 50 nT, in which we set a solenoid capable of producing magnetic fields up to ∼200 μT.

We tested four different initial conditions: AF-demagnetization, ARM, thermal demagnetization, and TRM. The TRM initial-state closely approximates conditions in nature for zero-age igneous/volcanic rocks. Because ARM is frequently used as a proxy for TRM, the ARM initial-state is of interest as well. Although irrelevant in nature, initial-states of AF and thermal demagnetizations are worth studying in order to make a fair comparison with the results in the literature. TRM was produced along z (cylindrical axis of the specimen) by cooling from 600 °C in a laboratory field $\mathbf{B} = 100\ \mu$T. ARM was imparted along z in an AF decaying from 100 mT with a superimposed steady field $\mathbf{B} = 100\ \mu$T. Similarly, cooling from 600 °C and AF decaying from 100 mT in zero-field ($\mathbf{B} = 0$) constitute thermal demagnetization and AF-demagnetization initial-states, respectively.

For each sample, we used three sister specimens in order to test the angular dependence in VRM acquisition. VRM was produced parallel (||), anti-parallel (\\), and orthogonal (⊥) to the cylindrical axis (z) of the sample (Fig. 3). To produce viscous remanence, samples were placed in-field $\mathbf{B} = 100\ \mu$T for various lengths of time, depending on experimental requirements (Fig. 3). The samples were periodically removed from the field to measure the remanence in zero-field, and then were quickly restored. Between successive measurements, the samples were oriented carefully so that the subsequent VRM acquisition would be in the same direction as the previous setting. This measurement and restoration procedure usually took <30 s.

The first set of experiments that simulated different initial-states, we monitored VRM acquisition for 2 weeks at room temperature. During this first run, VRM acquisition was measured at 1, 3, 6 h, 1, 3, 6, 10 and 13 days. Then, we repeated the same experiment, but measurement was carried out only after 13 days. We denote the second set of experiments as VRM*. Any difference between VRM and VRM* will reveal the influence of frequent sample removal/restoration in VRM acquisition. Overall, the entire experiment took 4 months to complete ([2 weeks for VRM + 2 weeks for VRM*] × 4 different initial-states).

One very important factor in VRM acquisition is the delay time (Δt), which is the elapsed time since the last magnetic treatment (Tivey and Johnson, 1981, 1984). We are not testing the Δt effect in the present study. For convenience, we used $\Delta t = 0$ in the present study.

5. Results

5.1. Angular dependence and initial-state dependence

Typical VRM acquisition experiments for various initial-states are shown in Fig. 4. All the values are normalized to the TRM intensity of the corresponding

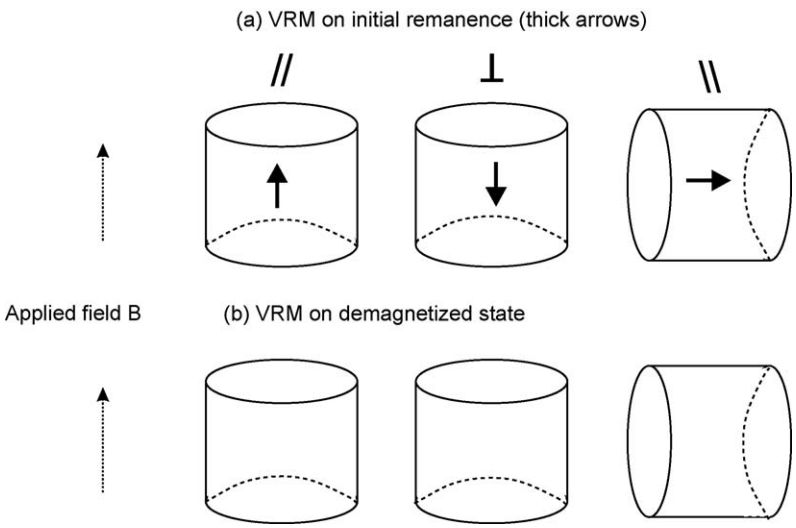

Fig. 3. An illustration of experimental design to produce VRM parallel (z), anti-parallel ($-z$), and orthogonal (x) to cylindrical axis (z) of the sample. VRM will be superimposed (a) on initial remanence of ARM or TRM and (b) on zero remanence of AF-demagnetization or thermal demagnetization. Dashed arrow: applied field; solid arrow: remanence direction.

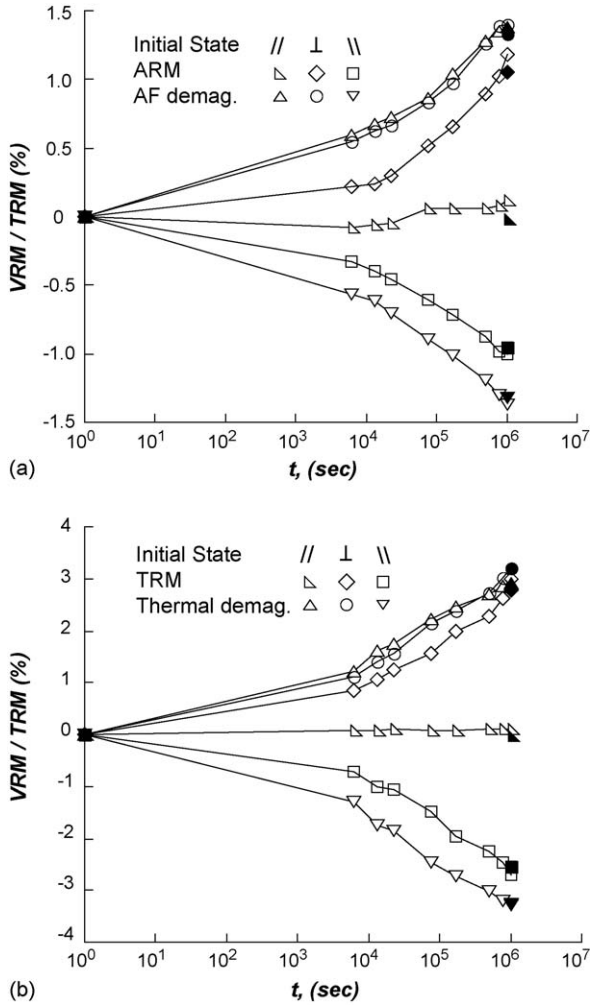

Fig. 4. VRM acquisition curves for various initial conditions. (a) AF-demagnetization and ARM states; (b) TRM and thermal demagnetization states. Open symbols: VRM; solid symbols: VRM*. Note that the growth of VRM is distinctly non-linear regardless of samples and various experimental conditions. The magnitude of VRM acquisition is nearly twice as large for the thermally treated initial conditions. In addition, the demagnetized initial-states were far more efficient at acquiring VRM than the initial remanence states.

specimen to make a fair comparison with the model in Fig. 1. Note also that the TRM was the ultimate equilibrium state (see Section 6). In our analysis, we set z (for parallel and anti-parallel results) and x (for perpendicular results) directions as positive axes for VRM growth (Fig. 3). Thus, VRM growth for the anti-parallel setting is represented as negative increase of magnetization (Fig. 3). We summarize typical features as follows:

(1) VRM, in general, steadily increases as time progresses with the exception of when **B** is parallel to an initial remanence. In a semi-log scale, the growth of VRM is distinctly non-linear over all time intervals $>10^4$ s regardless of samples and various experimental conditions (Fig. 4).
(2) A significant initial-state dependence is observed. The magnitude of VRM acquisition is nearly twice as large for the thermally treated initial conditions (compare Fig. 4a versus 4b). Moreover, the demagnetized initial-states were far more efficient at acquiring VRM than the initial remanence states (Fig. 4).
(3) The angular dependence of VRM acquisition is also dependent on the initial-state. For the same demagnetized states, VRM acquisition is insensitive to the applied field direction. Note that the VRM acquisition along the three directions is virtually identical from one another in terms of absolute scale. On the other hand, both ARM and TRM initial-states show a strong angular dependence. In particular, VRM acquisition for the parallel setting is insignificant (Fig. 4).
(4) There is a tendency for VRM to be larger than VRM* for all the specimens regardless of their initial-states and angular relations (e.g., solid symbols in Fig. 4).

5.2. Grain-size dependence

Testing the grain-size dependence of VRM acquisition using synthetic samples shows three interesting features (Fig. 5). First, "PSD" grains are the least efficient in acquiring VRM. Second, VRM acquisition patterns

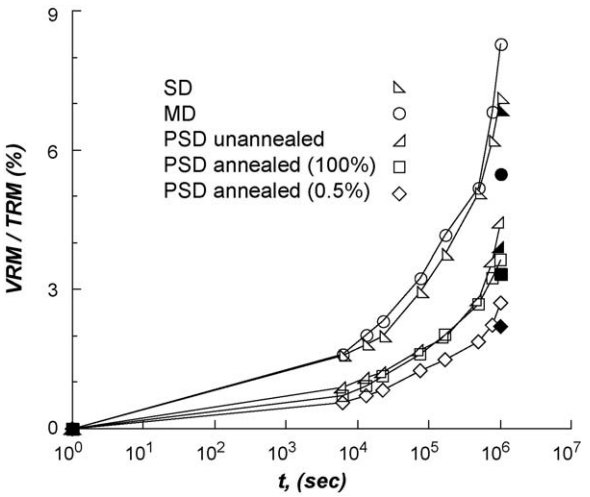

Fig. 5. Grain-size dependence of VRM acquisition. Note that PSD is least sensitive in VRM acquisition. There is a tendency for VRM to be larger than VRM* in MD. The annealing condition appears to affect the VRM acquisition process but a difference in volume concentration makes virtually no impact.

of the SD and MD grains appear similar. However, a discrepancy between VRM* and VRM is evident only for MD. Third, a difference in volume concentration appears to affect the VRM acquisition process but the annealing condition makes virtually no impact (Fig. 5).

6. Discussion

In the present study, we have tested the angular dependence, grain-size dependence, log(t) dependence, and the effect of initial magnetic state of sample on VRM acquisition. Consistent with SD theory, but contrary to most interpretations in the paleomagentic literature, a simple log-linear relationship between VRM acquisition and time t is not observed for any of our experiments (Figs. 4 and 5). This non-linear trend agrees well with our prediction (Fig. 1) and with previous long-term studies (e.g., Fig. 2). In particular, VRM acquisition is definitely non-linear even for a time intervals of a few hours. In fact, a log(t) dependence has only rarely been documented in the past (e.g., Shimizu, 1960). Instead, the characteristics of VRM acquisition are generally curved (e.g., Lowrie and Kent, 1978; Tivey and Johnson, 1981, 1984; Dunlop, 1983; Gee et al., 1993; Kelso and Banerjee, 1994). Despite the distinctly non-linear log(t) behavior from experiment and theory, calculating the S_a (viscous acquisition coefficient) over a short time interval has been a common practice. However, our results clearly indicate that this is likely to be highly misleading and resulting value S_a would depend strongly on the arbitrary selection of time intervals (Figs. 4 and 5). Furthermore, the angular-dependence and initial-state dependence cannot be properly incorporated in such estimations. Therefore, calculating a coefficient for log(t) dependence appears inadvisable.

We have modeled the simplest case where τ is narrowly confined with a mean of $\tau \sim 1$ s. In practice, natural rocks contain magnetic grains whose τ's are much larger (fortunately) and span several orders of magnitude. Yet, our simple calculation qualitatively predicts a non-linear log(t) dependence. Because VRM is still increasing after a 2-week long experiment, it is likely that our experiment covers only the tiny fraction of lower left margin in Fig. 1b. Considering the narrowness of the $f(\tau)$ that is activated in a laboratory time scale at room temperature, it is difficult to observe the entire behavior in Fig. 1b, although it is clearly evident in the very long-term experiment of Lowrie (1974; see Fig. 2). On the other hand, magnetic viscosity increases as the temperature rises (see Eq. (2)). Thus, the entire process in Fig. 1b would be reproducible over shorter time intervals at higher temperatures. Determining $f(\tau)$ from VRM acquisition at high temperatures will be the topic of a future paper.

VRM acquisition is strongly dependent on the initial magnetic state of the sample. In terms of absolute scale, the efficiency of VRM acquisition is ranked in the following order: thermal demagnetization, TRM, AF-demagnetization, and ARM (Fig. 4). We observed such trends in all samples regardless of their domain states. For comparative zero-field versus in-field settings (ARM versus AF-demagnetized or TRM versus thermal demagnetization), in-field conditions always yielded a lower efficiency in VRM acquisition (Fig. 4). A similar pattern of initial-state dependence has been documented for non-SD samples (e.g., Tivey and Johnson, 1981, 1984; Kelso and Banerjee, 1994). These results match well with magnetic domain observations for Ti-rich titanomagnetites (Halgedahl, 1991), where fewer domain walls were observed after thermal treatment. However, an opposite trend of higher efficiency in acquiring VRM on AF-demagnetization over TRM initial-state was once reported for synthetic SD samples (Tivey and Johnson, 1984).

The angular dependence of VRM acquisition has been generally ignored in the literature. For ARM and TRM initial-states, VRM growth is very low for the parallel case (Fig. 3). This interesting behavior originates from the fact that initial remanence condition is already an equilibrium state for parallel setting. Because $\mathbf{M}_{eq} = \mathbf{M}_0$, there is no room for any viscous change. In the parallel case, a TRM initial-state shows no increases of magnetization, indicating that TRM is a true equilibrium state. On the other hand, the ARM initial-state displays a slight increase of magnetization, suggesting that ARM is not as perfect equilibrium state as in TRM. Of course, this entire equilibrium argument is strictly applicable only when intensities of $\mathbf{B}$ to produce VRM and TRM (or ARM) are identical, as in our experiments. One can easily anticipate that VRM acquisition would be positive only for $\mathbf{B}_{VRM} > \mathbf{B}_{TRM}$. Nonetheless, estimating the cumulative viscous effect over geologic time requires a cautious approach in order to properly incorporate the effect of the angular dependence.

Values of VRM (samples removed from the field for measurements) were larger than VRM* (samples left in the field and only measured once) for samples containing coarse-grained magnetites (Fig. 5). In particular, there is a substantial difference between VRM and VRM* for MD samples (Fig. 5). We compiled all the values of VRM and VRM* for synthetic samples of field-treated (AF-demagnetization and ARM) initial-states (Fig. 6). If VRM is independent of sequential removal/restoration of

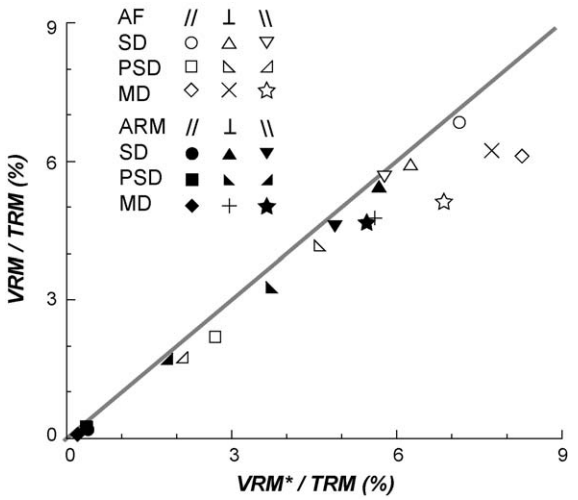

Fig. 6. Comparison of VRM and VRM*. Apart from the MD samples, the data points are quite linear, only slightly displaced from the grey ideal line. However, VRM was more intense than the VRM* in MD.

samples, VRM* should be identical to VRM. Apart from the MD samples, the data points are quite consistent, only slightly displaced from the ideal line (Fig. 5). However, the MD samples show that removal from zero-field condition (for measurements) and restoration to in-field condition (for VRM acquisition) apparently increased the efficiency of VRM acquisition (Figs. 5 and 6). Removal of the sample, even briefly, would have caused viscous decay, therefore a decrease in VRM. However, systematically more intense VRM than VRM* indicates that each removal/restoration sequence resets the equilibrium states in MD grains, promoting more acquisition of VRM. However, this proposition remains to be shown using micromagnetic simulation in a future study.

We also observed a grain-size dependence of VRM acquisition whereby VRM acquisition is least efficient in the PSD range. The much more efficient VRM acquisition in SD and MD have different physical origins, however. VRM acquisition in SD grains can be understood as a progressive blocking of the superparamagnetic

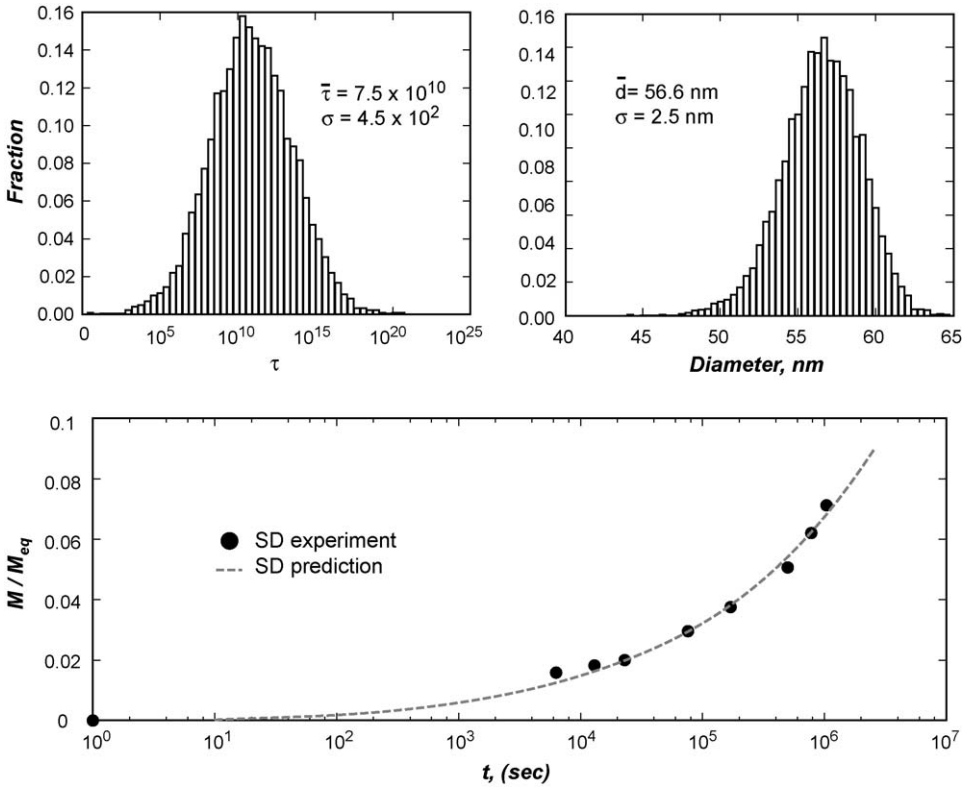

Fig. 7. VRM acquisition of SD magnetite grains. Our experimental observation for SD magnetite is best fit with a simple log-normal distribution of $\bar{\tau} = 7.5 \times 10^{10} \pm 4.5 \times 10^{2}$, which is equivalent to a grain-size distribution of 56.6 ± 2.5 nm if we use the following parameters: $\tau_0 = 10^{-10}$ s, $B_c = 10$ mT, effective grain diameter $= (6 \times \text{volume}/\pi)^{1/3}$, and $M_s(T_B) = 0.9 \times M_s(T_B)_{\text{magnetite}}$. We assumed 90% of saturation magnetization because of partial surface-oxidation of SD magnetite.

(SP)–SD grains. Because of the existing broad grain-size distribution in the synthetic and natural magnetites, there is frequently a fraction of magnetites whose sizes are near the SP–SD limit. While these magnetite grains cannot contribute to the initial magnetization, they gradually contribute to VRM acquisition. On the other hand, enhanced VRM acquisition capacity in MD possibly results from domain wall reconfigurations.

How well can the modeling predict the VRM acquisition? Our experimental observation for SD magnetite is best fit with a simple log-normal distribution of $\bar{\tau} = 7.5 \times 10^{10} \pm 4.5 \times 10^{2}$, which is equivalent to a grain-size distribution of 56.6 ± 2.5 nm (Fig. 7). The minor discrepancy between the best-fitting estimation and actual observation may result from various physical sources. First, the observed grain-size distribution is much broader (65 ± 36 nm) than that in the model. Second, there is a morphologic difference of magnetite between the modeling and observation. For instance, the modeled grain-size distribution assumed cubic morphology while the observed magnetites were rectangular in cross section with average aspect ratio (=major/minor axes) of 1.48 (Yu et al., 2002; Table 1). Third, there is an inherent uncertainty in using two-dimensional photos collected from scanning electron microscopy (Kong et al., 2005). Fourth, it is possible that the surface of SD magnetite was slightly oxidized into maghemite, thus reduced the saturation magnetization.

7. Conclusions

(1) Contrary to traditional VRM interpretation, we observed a highly non-linear log(t) dependence of VRM acquisition for all the samples used in the present study regardless of various experimental conditions.
(2) VRM acquisition is strongly dependent on the initial magnetic state of the samples. We observed a higher efficiency of VRM acquisition in the following order: thermal demagnetization, TRM, AF-demagnetization, and ARM.
(3) We found an angular dependence of VRM acquisition. In particular, when VRM is produced in a direction parallel to the direction of the initial thermal or anhysteretic remanence, VRM acquisition is negligible.
(4) There is a tendency for VRM (that was removed from the field for measurements) to be larger than VRM* (that was left in the field and only measured once) for samples containing coarse-grained magnetites. In MD magnetites, frequent removal and restoration of samples (for the purpose of zero-field remanence measurement) apparently increased the efficiency of VRM acquisition.
(5) Grain-size dependence of VRM acquisition using synthetic samples shows that magnetite in the PSD range are the least sensitive to viscous remanence acquisition, as initially documented by Dunlop (1983).

Acknowledgments

This research was supported by NSF grant EAR0229498 to L. Tauxe. We thank Jason Steindorf for help with the measurements. Helpful reviews by William Lowrie and an anonymous referee improved the paper.

References

Bina, M.M., Henry, B., 1990. Magnetic properties, opaque mineralogy and magnetic anisotropies of serpentinized peridotites from ODP Hole 670 A near the mid-Atlantic ridge. Phys. Earth Planet. Int. 65, 88–103.

Bina, M.M., Prévot, M., 1994. Thermally activated magnetic viscosity in natural multidomain Titanomagnetite. Geophys. J. Int. 117, 495–510.

Biquand, D., Prévot, M., 1971. AF demagnetization of viscous remanent magnetization in rocks. Zeit. Geophy. 37, 471–485.

Bowles, J.A., Johnson, H.P., 1999. Behavior of oceanic crustal magnetization at high temperatures: viscous magnetization and the marine magnetic anomaly source layer. Geophys. Res. Lett. 26, 2282–2779.

Creer, K.M., Petersen, N., Petherbridge, J., 1970. Partial self-reversal of remanent magnetization and anisotropy of viscous magnetization in basalts. Geophys. J. R. Astro. Soc. 21, 471–483.

Dunlop, D.J., 1973. Theory of the magnetic viscosity of lunar and terrestrial rocks. Rev. Geophys. Space Phys. 11, 855–901.

Dunlop, D.J., 1983. Viscous magnetization of 0.04–100 μm magnetites. Geophys. J. R. Astro. Soc. 74, 667–687.

Dunlop, D.J., Hale, C.J., 1977. Simulation of long-term changes in the magnetic signal of the oceanic crust. Can. J. Earth Sci. 14, 716–744.

Dunlop, D.J., Özdemir, Ö., 1997. Rock Magnetism: Fundamentals and Frontiers. Cambridge University Press, New York, p. 573.

Evans, M.E., Heller, F., 1994. Magnetic enhancement and paleoclimate: study of a loess/paleosol couplet across the Loess Plateau of China. Geophys. J. Int. 117, 257–264.

Gaunt, P., 1986. Magnetic viscosity and thermal activation energy. J. Appl. Phys. 59, 4129–4132.

Gee, J.S., Tauxe, L., Hildebrand, J.A., Staudigel, H., Lonsdale, P., 1988. Non-uniform magnetization of Jasper Seamount. J. Geophys. Res. 93, 12159–12175.

Gee, J.S., Staudigel, H., Tauxe, L., Pick, T., Gallet, Y., 1993. Magnetization of the La Palma Seamount series: implications for Seamount paleopoles. J. Geophys. Res. 98, 11743–11767.

Halgedahl, S.L., 1991. Magnetic domain patterns observed on synthetic Ti-rich titanomagnetite as a function of temperature and in states of thermoremanent magnetization. J. Geophys. Res. 96, 3943–3972.

Hall, J.M., Walls, C.C., Hall, S.L., 1995. Viscous magnetization at 300 K in a profile through Troodos type oceanic crust. Phys. Earth Planet. Int. 88, 101–116.

Jackson, M.J., 1990. Diagenetic sources of stable remanence in remagnetized Paleozoic cratonic carbonates: a rock magnetic study. J. Geophys. Res. 95, 2753–2762.

Jackson, M.J., Van der Voo, R., 1986. Thermally activated viscous remanence in some magnetite- and hematite-bearing dolomites. Geophys. Res. Lett. 13, 1434–1437.

Jackson, M.J., Worm, H.-U., 2002. Anomalous unblocking temperatures, viscosity and frequency-dependent susceptibility in the chemically-remagnetized Trenton limestone. Phys. Earth Planet. Int. 126, 27–42.

Kelso, P.R., Banerjee, S.K., 1994. Elevated temperature viscous remanent magnetization of natural and synthetic multidomain magnetite. Earth Planet. Sci. Lett. 122, 43–56.

Kent, D.V., 1985. Thermoviscous remagnetization in some Appalachian limestones. Geophys. Res. Lett. 12, 805–808.

Kent, D.V., Miller, J.D., 1987. Redbeds and Thermoviscous magnetization theory. Geophys. Res. Lett. 14, 327–330.

Kligfield, R., Channell, J.E.T., 1981. Widespread remagnetization of Helvetic limestones. J. Geophys. Res. 86, 1888–1900.

Kok, Y.S., Tauxe, L., 1996a. Saw-tooth pattern of relative paleointensity records and cumulative viscous remanence. Earth Planet. Sci. Lett. 137, 95–99.

Kok, Y.S., Tauxe, L., 1996b. Saw-toothed pattern of sedimentary paleointensity records explained by cumulative viscous models. Earth Planet. Sci. Lett. 44, E9–E14.

Kong, M., Bhattacharya, R.N., James, C., Basu, A., 2005. A statistical approach to estimate the 3D size distribution of spheres from 2D size distributions. Geol. Soc. Am. Bull. 117, 244–249.

Lawrence, R.M., Gee, J.S., Karson, J.A., 2002. Magnetic anisotropy of serpentinized peridotites from the MARK area: implications for the orientation of mesoscopic structures and major fault zones. J. Geophys. Res. 107 (B4), 2073, doi:10.1029/2000JB000007.

Le Goff, M., Gallet, Y., 2004. A new three-axis vibrating sample magnetometer for continuous high-temperature magnetization measurements: applications to paleo- and archeo-intensity determinations. Earth Planet. Sci. Lett. 229, 31–43.

Lowrie, W., 1973. Viscous remanent magnetization in oceanic basalts. Nature 243, 27–30.

Lowrie, W., 1974. Oceanic basalt magnetic properties and the Vine Mattews hypothesis. J. Geophys. 40, 515–536.

Lowrie, W., Kent, D.V., 1976. Viscous remanent magnetization in basalt samples. Init. Rep. Deep Sea Drill. Proj. 34, 479–484.

Lowrie, W., Kent, D.V., 1978. Characteristics of VRM in oceanic basalts. J. Geophys. 44, 297–315.

Markert, H., Heller, F., Steigenberger, N., 1976. Parabolic field dependence of kinks occurring in the logarithmic time plots of viscous magnetization. J. Geophys. 42, 47–58.

Moskowitz, B., 1985. Magnetic viscosity, diffusion after-affect, and disaccommodation in natural and synthetic samples. Geophys. J. R. Astro. Soc. 82, 143–161.

Moskowitz, B., Banerjee, S.K., 1981. A comparison of the magnetic properties of synthetic titanomagnetites and some oceanic basalts. J. Geophys. Res. 86, 11869–11882.

Muxworthy, A.R., Williams, W., 2006. Observation of viscous magnetization in multidomain magnetite. J. Geophys. Res. 111, B01103, doi:10.1029/2005JB003902.

Nagata, T., Carleton, B.J., 1970. Natural remanent magnetization and viscous magnetization of Apollo 11 lunar materials. J. Geomag. Geoelec. 22, 491–506.

Néel, L., 1949. Théorie du traînage magnétique des ferromagnéniques en grains fins avec applications aux terres cuites. Ann. Géeophys. 5, 99–136.

Néel, L., 1950. Théorie du traînage magnétique des substances massives dans la domaine de Rayleigh. J. Phys. Radium 11, 49–61.

Néel, L., 1955. Some theoretical aspects of rock magnetism. Adv. Phys. 4, 191–243.

Özdemir, Ö., Banerjee, S.K., 1981. An experimental study of magnetic viscosity in synthetic monodomain titanomaghemites: implications for the magnetization of oceanic crust. J. Geophys. Res. 86, 11864–11868.

Pan, Y., Zhu, R., Shaw, J., Liu, Q., Guo, B., 2001. Can relative paleointensities be determined from the normalized magnetization of the wind-blown loess of China? J. Geophys. Res. 106, 19221–19232.

Prévot, M., 1981. Some aspects of magnetic viscosity in subaerial and submarine volcanic rocks. Geophys. J. R. Astro. Soc. 66, 169–183.

Prévot, M., Bina, M.M., 1993. Origin of magnetic viscosity and estimate of long-term induced magnetization in coarse-grained submarine basalts. Geophys. Res. Lett. 20, 2483–2486.

Pozzi, J.P., Dubuisson, G., 1992. High temperature viscous magnetization of oceanic deep crustal- and mantle-rocks as a partial source for MAGSAT magnetic anomalies. Geophys. Res. Lett. 19, 21–24.

Rimbert, F., 1959. Contribution à l'étude de l'action de champs alternatifs sur les aimantations rémanentes des roches. Applications géophysiques. Rev. Institut Franc. Pétrole. 14, 17–54.

Shimizu, Y., 1960. Magnetic viscosity of magnetite. J. Geomag. Geoelec. 11, 125–138.

Smith, B.M., 1984. Magnetic viscosity of some doleretic basalts in relation to the interpretation of the oceanic magnetic anomalies. Geophys. Res. Lett. 11, 213–216.

Smith, R.T., Verosub, K.L., 1994. Thermoviscous remanent magnetism of Columbia river basalt blocks in the Cascade landslide. Geophys. Res. Lett. 21, 2661–2664.

Sporer, H., 1984. On viscous remanent magnetization of synthetic multidomain titanomagnetite. Geophys. Res. Lett. 11, 209–212.

Tivey, M., Johnson, H.P., 1981. Characterization of viscous remanent magnetization in single- and multi-domain magnetite grains. Geophys. Res. Lett. 8, 217–220.

Tivey, M., Johnson, H.P., 1984. The characterization of viscous remanent magnetization in large and small magnetite particles. J. Geophys. Res. 89, 543–552.

Walton, D., 1980. Viscous magnetization. Nature 286, 245–247.

Williams, W., Walton, D., 1986. Demagnetization of viscous moments. Geophys. J. Roy. Astro. Soc. 74, 667–687.

Williams, W., Walton, D., 1988. Thermal cleaning of viscous magnetic moments. Geophys. Res. Lett. 15, 1089–1092.

Williams, W., Muxworthy, A.R., 2006. Understanding viscous magnetization of multidomain magnetite. J. Geophys. Res. 111, B02102, doi:10.1029/2005JB003695.

Worm, H.-U., 2001. Magnetic stability of oceanic gabbros from ODP Hole 735 B. Earth Planet. Sci. Lett. 193, 287–302.

Worm, H.-U., Jackson, M., Kelso, P., Banerjee, S.K., 1988. Thermal demagnetization of partial thermoremanent magnetization. J. Geophys. Res. 93, 12196–12204.

Yamazaki, T., 1986. Secondary remanent magnetization of pelagic clay in the south Pacific: application of thermal demagnetization. Geophys. Res. Lett. 13, 1438–1441.

Yamazaki, T., Katsura, I., 1990. Magnetic grain size and viscous remanent magnetization of pelagic clay. J. Geophys. Res. 95, 4373–4382.

Yu, Y., Rock magnetic and palaeomagnetic experiments on hemoilmenites and titanomagnetites in some volcanic rocks from Japan. M.Sc. Thesis. University of Toronto, 1998, p. 24.

Yu, Y., Dunlop, D.J., 2001. Paleointensity determination on the late Precambrian Tudor Gabbro, Ontario. J. Geophys. Res. 106, 26244–26331.

Yu, Y., Dunlop, D.J., 2002. Multivectorial paleointensity determination from the Cordova Gabbro, southern Ontario. Earth Planet. Sci. Lett. 203, 983–998.

Yu, Y., Dunlop, D.J., Özdemir, Ö., 2002. Partial anhysteretic remanent magnetization in magnetite. 1. Additivity. J. Geophys. Res. 107 (B10), 2244, doi:10.1029/2001JB001249.